RSC Advances

PAPER

View Article Online
View Journal | View Issue

Cite this: *RSC Adv.*, 2021, **11**, 27969

A comparative study on the coordination of diglycolamide isomers with Nd(III): extraction, third phase formation, structure, and computational studies†

Yaoyang Liu,[a] Sheng Liu,[a] Zhibin Liu,[a] Chuang Zhao,[a] Chunhui Li,[a] Yu Zhou,[a] Caishan Jiao,[a] Yang Gao,[*a] Hui He[*ab] and Shaowen Zhang[c]

A novel asymmetric diglycolamide *N*,*N*-dimethyl-*N*′,*N*′-dioctyl diglycolamide (L^{II}) was synthesized. The Nd(III) extraction behavior from HNO_3 and loading capability of the solution of L^{II} in 40/60 (v/v)% *n*-octanol/kerosene were studied. Analyses by the slope method, ESI-MS, and FT-IR indicated that, similar to the previously studied isomer ligand *N*,*N*′-dimethyl-*N*,*N*′-dioctyl diglycolamide (L^{I}), 1 : 3 Nd(III)/L^{II} complexes formed. Under the same experimental conditions, the distribution ratio and limiting organic concentration of L^{II} towards Nd(III) were smaller than those of L^{I}, but the critical aqueous concentration of L^{II} was larger, which implies that L^{II} exhibited poorer extraction and loading capabilities towards Nd(III) than L^{I}, and L^{II} has a tendency to be less likely to form the third phase. The quasi-relativistic density functional theory (DFT) calculation was performed to provide some explanations for the differences in their extraction behaviors. The electrostatic potential of the ligands indicated that the electron-donating ability of the amide O atoms in L^{II} displayed certain differences compared with L^{I}. This inhomogeneity in L^{II} affected the interaction between L^{II} and Nd(III), as supported by QTAIM and bonding nature analysis, and it seemed to reflect in the extraction performance towards Nd(III).

Received 31st May 2021
Accepted 21st July 2021

DOI: 10.1039/d1ra04222j

rsc.li/rsc-advances

Introduction

In order to meet the growing demand for energy and combat climate change, many countries have put forward the strategy of developing nuclear power. However, the treatment and disposal of radioactive waste, especially high-level liquid waste (HLLW) generated from spent fuel reprocessing, has always been a challenging and controversial issue associated with the sustainable use of nuclear fuels. Minor actinides (MAs) and long-lived fission product (FP) radionuclides are separated from HLLW and then incinerated into short-lived nuclides in nuclear reactors or accelerators, and this process is called partitioning & transmutation (P&T).[1] Thus, the radiotoxicity and volume of HLLW can be decreased significantly. In the past few decades, diglycolamides (DGAs, Fig. 1) have been identified as one of the most up-and-coming extractants in the field of HLLW separation due to their strong affinity towards actinides (An) and lanthanides (Ln), which results in tridentate chelates with CHON compositions that are benign to the environment.[2]

DGAs can be divided into two categories, namely symmetric DGAs ($R_1 = R_2 = R_3 = R_4$) and asymmetric DGAs (structure **A:** $R_1 = R_3$, $R_2 = R_4$ or structure **B:** $R_1 = R_2$, $R_3 = R_4$) on the basis of the alkyl substituent attached to the N atom of amide. *N*,*N*,*N*′,*N*′-Tetraoctyl diglycolamide (TODGA)[3–5] and *N*,*N*,*N*′,*N*′-tetra(2-ethylhexyl) diglycolamide (TEHDGA) are the most extensively studied DGAs and have been applied in several HLLW separation processes.[6,7] However, they suffer the problem of third phase formation in the extraction process. Although adding phase modifiers, such as tributyl phosphate (TBP), *N*,*N*-dihexyl

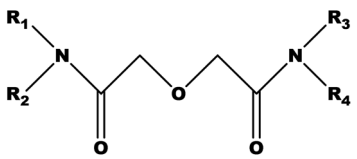

Fig. 1 The structure of DGA (R_1–R_4 are alkyl groups).

[a]*Fundamental Science on Nuclear Safety and Simulation Technology Laboratory, College of Nuclear Science and Technology, Harbin Engineering University, Harbin, Heilongjiang Province, China, 150001. E-mail: gaoyang@hrbeu.edu.cn*

[b]*China Institute of Atomic Energy, P. O. Box 275 (126), Beijing, 102413, China. E-mail: hehui@ciae.ac.cn*

[c]*School of Chemistry and Chemical Engineering, Key Laboratory of Cluster Science of Ministry of Education, Beijing Institute of Technology, Beijing, 100081, China*

† Electronic supplementary information (ESI) available: Characterization data of L^{II} by ^{1}H NMR, ^{13}C NMR and FT-IR; effect of NO_3^- and H^+ concentration on D_{Nd}; effect of temperature on the *K*; LOC of Nd(III) as a function of aqueous phase acidity and ligand concentration; stripping behavior; Mulliken charge population analysis; average Nd–O bond lengths of complexes. See DOI: 10.1039/d1ra04222j

octyl amide (DHOA), and *n*-octanol, can increase the metal loading capacity of the extractant, this adjustment complicates the solvents and causes more fission products like Zr(IV) and Mo(VI) to proceed to the organic phase.[8] It was found that some asymmetric DGAs, such as *N*,*N*-di(2-ethylhexyl)-*N*′,*N*′-dioctyl diglycolamide and *N*,*N*-didecyl-*N*′,*N*′-dioctyl diglycolamide,[9,10] improved the performance to a certain extent by inhibiting third phase formation, as well as extraction performance, and selectivity for An(III) and Ln(III). For example, *N*,*N*-didodecyl-*N*′,*N*′-dioctyl diglycolamide displayed the advantages of a high distribution ratio of Nd(III) and no third phase formation with Nd(III) even at the initial concentration of 600 mM in 3 to 4 M nitric acid medium.[11] *N*,*N*-Dihexyl-*N*′,*N*′-didecyl diglycolamide could separate Ln(III) from Fe(III), Ni(II), Co(II) and Cs(I) effectively.[12] *N*,*N*′-Dimethyl-*N*,*N*′-dioctyl diglycolamide exhibited the high LOC (the limiting organic concentration) and CAC (the critical aqueous concentration) of Nd(III) in nitric acid and considerably good extraction ability towards actinide and lanthanide ions with various oxidation states, such as Nd(III), Pu(IV), Np(V), and U(VI).[13–17] These asymmetric DGAs are supposedly superior ligands for the separation of An(III)/Ln(III) from HLLW.

Although asymmetric DGAs have obtained extensive attention, most studies have focused on one type of asymmetric DGAs, either the **A** or **B** structure, while a few studies involve the comparison of the two types of asymmetric DGAs in terms of the loading capacity of acid and metal ions, and extraction behaviors, as well as separation performances. The two types of asymmetric DGAs differ in many characteristics, such as electron donor ability, space steric hindrance and coordination ability, which probably affect the interaction strength between metal ions and the ligands. Both theoretical and experimental studies on DGA-type or DAPhen-type soft ligands have shown that the subtle steric and electronic charge variations markedly affect the structure–activity relationship of the ligands,[18–20] which is ultimately reflected in the metal-ion extraction performance. In this study, neodymium, a typical member of the lanthanide series, was selected as the target element because, on the one hand, high-level radioactive waste contains a large proportion of lanthanides (~45%), and on the other hand, it has often been used as the research object in the formation of the third phase.[22] Two types of DGAs (Fig. 2), *N*,*N*′-dimethyl-*N*,*N*′-dioctyl diglycolamide (L^I) and *N*,*N*-dimethyl-*N*′,*N*′-dioctyl diglycolamide (L^{II}), were used as the extractants, and the differences in their extraction performance, extraction thermodynamics, and loading capabilities towards Nd(III) were investigated through extraction experiments, in conjunction with the scalar-relativistic theoretical method.

Experimental methods

Materials

Diglycolic anhydride (98%), dioctylamine (95%), dimethylamine in tetrahydrofuran (THF) (2 M), isobutyl chloroformate (IBCF, 98%), 4-methylmorpholine (NMM, 98%), neodymium nitrate hexahydrate (99.9%) were supplied by Aladdin Industrial Corporation. The other chemicals (analytical grade) were supplied by Sinopharm Reagent Co., Ltd.

Synthesis

The ligand L^I was synthesized by two-step method.[21] The ligand L^{II} was synthesized by a mixed anhydride method.[23] The synthetic route of L^{II} is depicted in Fig. 3. A brief description of the synthesis steps is given below:

Dioctyldiglycolamic acid (**3**, DODGAA) was first synthesized by the reaction between diglycolic anhydride (**1**) and dialkylamine (**2**).[9] A mixture of 0.03 mol DODGAA dissolved in 150 mL THF and 0.03 mol *N*-methylmorpholine was stirred in an ice brine bath. When the temperature dropped to −10 °C, a mixture of 3.8 mL (0.03 mol) isobutyl chloroformate and THF (volume ratio 1 : 1) was slowly added. Then, 15 mL dimethylamine in THF (**4**, 2 M) was added dropwise at −2 °C. Excess THF was evaporated under reduced pressure. After washing, filtering, rotary evaporation and separation on a silica gel column, the target product L^{II} ligand (**5**) was obtained with a yield of 80%. Characterization data from ^{1}H NMR, ^{13}C NMR and FT-IR spectroscopy are presented in the ESI.†

Solvent extraction and third phase formation

The aqueous solution containing Nd(III) and the organic phase were mixed in equal volumes for 30 min at 25 ± 0.2 °C (s100 oscillator, Dianshan Lake Instrument Company, Kunshan, Jiangsu, China). The equilibrium time experiments demonstrated that 30 min was enough for the two phases to reach equilibrium. The two phases were then separated by centrifugation (LG16B high-speed centrifuge, Leiboer Medical Devices Co., Ltd., Beijing, China) at 2500 rpm for 10 min. The Nd(III) concentration in the raffinate was assayed by inductively coupled plasma mass spectroscopy (X-II ICP-MS, Thermo Fisher Scientific, Waltham, MA, USA). The Nd(III) concentration in the organic phase was determined by subtracting the Nd(III)

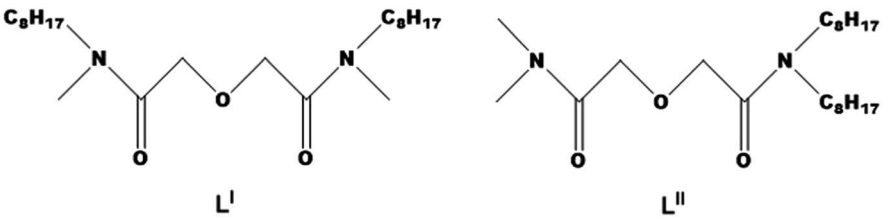

Fig. 2 The structures of the isomeric extractants studied in this paper.

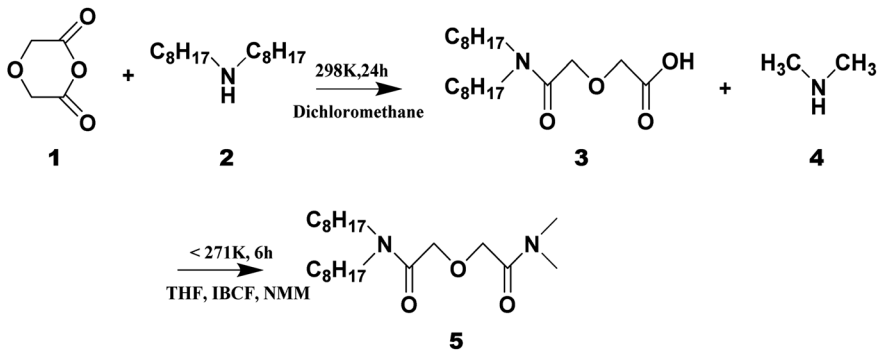

Fig. 3 Synthetic routes of the two extractants.

concentration in the raffinate from the initial aqueous Nd(III) concentration.

The distribution ratio, D_{Nd}, was derived from:

$$D_{Nd} = \frac{C_o}{C_a} = \frac{C - C_a}{C_a} \quad (1)$$

C, C_a, and C_o represent the initial concentration of Nd(III) in the aqueous phase and the concentrations of Nd(III) in the raffinate and organic phase after the extraction equilibrium, respectively. The acidity of the two phases after equilibrium was determined by acid–base titration with a standard NaOH solution. All data were obtained from three sets of parallel tests, and the error was below 5%.

Two parameters, LOC and CAC, are usually used for evaluating the third phase formation behavior.[24,25] The organic phase and the aqueous phase containing nitric acid or Nd(III) were mixed thoroughly in equal volume. The third phases formed by nitric acid and Nd(III) were yellowish-brown and light pink, respectively. Then, the third phase was dissolved cautiously by adding distilled water or the pre-equilibrated organic phase dropwise until it disappeared. The complexometric method and standard acid–base titration were used to determine the concentrations of Nd(III) and nitric acid in the organic and aqueous phases, respectively.[10,26,27] All data were obtained from three sets of parallel tests, and the error was below 5%.

ESI-MS methods

Mass spectrometric measurements were recorded in the positive-ion mode using a Bruker micrOTOF Q II (Bruker Daltonics, Bremen, Germany), and an electrospray interface was used as the ionization source. The solutions for ESI-MS measurements were prepared by adding a certain volume of the metal stock solution (2×10^{-2} M) to 5 mL of the ligand solution (5×10^{-4} M), and the ESI-MS spectra were obtained in the presence of excess extractant.

Infrared spectroscopy

The IR spectra of the extracted species were recorded on a Fourier Transform Infrared Spectrometer (Spectrum 100 FT-IR, Perkin Elmer, Waltham, MA, USA), and the detailed procedure has been described in a previous study.[26]

Theoretical calculations

The Gaussian 16 program package was used for structural optimization by DFT.[28–30] The three-parameter hybrid functional common formulation, B3LYP,[31,32] which has been demonstrated to produce reliable structural results for actinide and lanthanide complexes, was employed.[33,34] The 28 electron core pseudopotentials (ECPs) and the corresponding ECP28MWB-SEG valence basis sets were applied for Nd,[35–37] and the polarized 6-311G(d) basis set was used for the lighter atoms (H, C, N, and O).

All the geometrical parameters were optimized at the B3LYP/6-311G(d)/RECP level of theory in the gas phase. M052X/6-31G(d)/RECP[38] was chosen for the thermodynamics analysis based on the optimized molecular geometries to gain more accurate energies. Solvation effects were evaluated by the Solvation Model Based on Density (SMD) with the custom SMD mixing solvent parameters.[39]

The electrostatic potentials (ESP) and Mulliken charge population analysis of the two ligands were investigated. In order to understand the metal–ligand bonding properties, the Mayer bond order (MBO) was calculated at the same theory level,[40] and the quantum theory of atoms in molecules (QTAIM) parameters were explored at the bond critical points (BCPs) using the Multiwfn software version 3.7.[41–44]

Results and discussion

Solvent extraction

Effect of nitric acid concentration. Fig. 4 illustrates the trend of D_{Nd} at the concentrations of 0.5 M to 6.0 M HNO_3, and the results show that D_{Nd} first increased and then decreased slightly and that the maximum values of D_{Nd} appear at about 3.0 M HNO_3. The upward trend of the distribution ratio can be explained by the mass action law and the salting-out effect of NO_3^- with increasing HNO_3 concentration.[45,46] The competitive effect of H^+ suppresses the extraction of Nd(III). The effects of nitrate concentration and H^+ concentration on D_{Nd} are shown in Fig. S1 and S2.†

Effect of ligand concentration. The ligands L^I and L^{II} are neutral extractants,[47–49] and the equation for the extraction of Nd(III) by L^{II} can be expressed as:

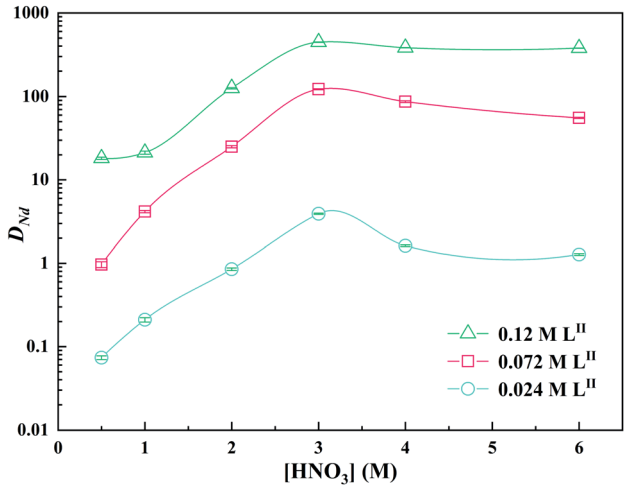

Fig. 4 D_{Nd} as a function of HNO_3 concentration, $[Nd^{3+}] = 3$ mM.

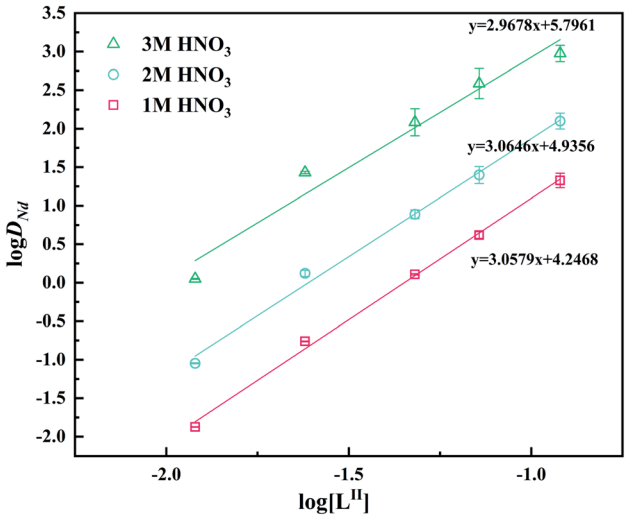

Fig. 5 D_{Nd} as a function of extractant concentration, $[Nd^{3+}]_{init} = 3$ mM, $[L^{II}] = 0.012–0.12$ M.

$$Nd_{(aq)}^{3+} + 3NO_{3(aq)}^{-} + nL^{II}_{(o)} \leftrightarrow Nd(NO_3)_3 \cdot nL^{II}_{(o)} \quad (2)$$

The extraction equilibrium constant K can be expressed as:

$$K = \frac{[Nd(NO_3)_3 \cdot nL^{II}]_{org}}{\gamma_{Nd^{3+}}\gamma_{NO_3^-}{}^3[Nd^{3+}]_{aq}[NO_3^-]_{aq}{}^3[L^{II}]_{org}{}^n}$$

$$= \frac{[Nd(NO_3)_3 \cdot nL^{II}]_{org}}{\gamma_{Nd(NO_3)_3}{}^4[Nd^{3+}]_{aq}[NO_3^-]_{aq}{}^3[L^{II}]_{org}{}^n}$$

$$= \frac{D_{Nd}}{\gamma_{Nd(NO_3)_3}{}^4[NO_3^-]_{aq}{}^3[L^{II}]_{org}{}^n} \quad (3)$$

The subscripts 'aq' and 'o' represent the aqueous phase and the organic phase, respectively. $[L^{II}]_{org}$ and $[Nd(NO_3)_3 \cdot nL^{II}]_{org}$ are the concentrations of the free extractant and the complex in the organic phase, respectively. $[Nd^{3+}]_{aq}$ and $[NO_3^-]_{aq}$ are the concentrations of Nd(III) and NO_3^- in the aqueous phase, respectively. $\gamma_{Nd^{3+}}$ and $\gamma_{NO_3^{3-}}$ are the ionic activity coefficients of Nd(III) and NO_3^-, respectively, $\gamma_{Nd(NO_3)_3}$ is the average ionic activity coefficient of $Nd(NO_3)_3$. The average activity coefficient $\gamma_{Nd(NO_3)_3}$ has been addressed using a simplified Pitzer model in mixed electrolyte solutions,[50–52] and the equations, related parameters, and the average activity coefficients at various temperatures for some lanthanides have been solved in our previous studies.[16]

The term D_{Nd} can be calculated as:

$$D_{Nd} = \gamma_{Nd(NO_3)_3}{}^4 K[NO_3^-]_{aq}{}^3[L^{II}]_{org}{}^n \quad (4)$$

Adjusting eqn (3) in the logarithmic form gives:

$$\lg D_{Nd} = n \lg[L^{II}]_{org} + \lg K\gamma_{\pm Nd(NO_3)_3}{}^4[NO_3^-]_{aq}{}^3 \quad (5)$$

The 'n' values obtained by slope analysis are shown in Fig. 5. As seen, the slopes are all around 3, indicating that the stoichiometric ratio of Nd(III) to L^{II} in the extracted species was 1 : 3. This result is similar to the previously published results.[53–56] Fig. 6 displays the ESI-MS of L^{I} and L^{II} ligands and their complexes with Nd(III). The characteristic peaks in the mass spectra of the two ligands are almost identical ([L^{I} + H$^+$, m/z 385.5; L^{II} + H$^+$, m/z 385.5]). When the ligands complexed with Nd(III), a peak appeared at m/z 681.6 corresponding to $[Nd + 3L^{I} + NO_3]^{2+}$/$[Nd + 3L^{II} + NO_3]^{2+}$. The structures of the complexes of L^{I} and L^{II} with Nd(III) could be identified as $[NdL^{I}_3]^{3+}$ and $[NdL^{II}_3]^{3+}$, respectively. Therefore, the compositions of the complexes formed by the two ligands and Nd(III) are the same.

Table 1 compares the Nd(III) extraction performances of the L^{I} and L^{II} ligands and lists the distribution ratios at different

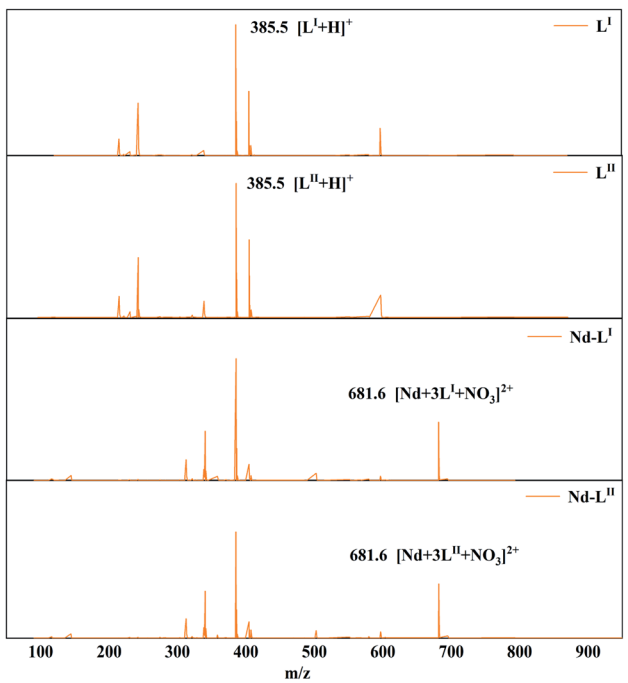

Fig. 6 ESI-MS analysis of the Nd(III) complexes with L^{I} and L^{II} in acetonitrile. M : L = 1 : 3; temperature: 25 ± 0.5 °C.

Table 1 D_{Nd} of L^I/L^{II} for Nd(III) extraction in *n*-octanol/*n*-dodecane at 298 K. The data for L^I are from a previous study[26]

		$[HNO_3]$ (M)				
Ligand	[L] (M)	1	2	3	4	6
L^I	0.024	0.80	2.72	4.81	4.40	3.99
	0.072	30.62	115.85	155.84	160.40	151.11
	0.12	117.94	306.42	490.55	466.24	347.20
L^{II}	0.024	0.21	0.85	3.92	1.62	1.27
	0.072	4.16	25.02	122.22	86.89	55.51
	0.12	21.23	125.61	446.37	382.76	379.01

concentrations of nitric acid and ligands. Under the same experimental conditions, the D_{Nd} of L^I is higher than that of L^{II}.

Thermodynamics of extraction. The thermodynamic data of the extraction process was obtained over the range of 298–333 K. According to the Vant'Hoff equation, the relationship between ΔG, ΔH, ΔS, K and T can be expressed as presented in eqn (6). The equilibrium constant K at each temperature is obtained by eqn (7). As shown in Fig. S3,† the plots of $\log K$ *vs.* $(1/T)$ are approximately linear, and the slope and intercept values can be used to calculate the values of ΔH and ΔS base on eqn (7).

$$\Delta G = \Delta H - T\Delta S = -2.303RT \lg K \quad (6)$$

$$\lg K = \lg \frac{D_{Nd}}{\gamma_{Nd(NO_3)_3}{}^4 [NO_3^-]_{aq}{}^3 [L^{II}]_{org}{}^3} = -\frac{\Delta H}{2.303RT} + \frac{\Delta S}{2.303R} \quad (7)$$

where T and R denote the absolute temperature and gas constant, respectively.

Table 2 lists the thermodynamic data of Nd(III) extraction with the L^{II} ligand, and the data of the L^I ligand is also included for comparison. The ΔG values of the two ligands are negative, implying that the two extraction processes are exothermic. The absolute value of $\log K$ of L^I is larger than that of L^{II}, which means that Nd(III) is more prone to complexation with L^I ligand than with L^{II} ligand at 298 K. The negative values of ΔS is because the degree of disorder in the extraction systems is reduced by the formation of the extracted species.[57] The thermodynamic data on the extraction reaction combined with the results of the D_{Nd} demonstrates that the L^I ligand has better Nd(III) extraction capability.

Stripping studies of Nd(III). Dilute nitric acid is considered as a better stripping agent For DGA extractants.[58,59] In our previous studies, 0.001 M nitric acid is highly effective in stripping and is more effective in light lanthanides.[16] The effect of nitric acid concentration on the stripping efficiency of the organic phase of the L^{II} ligand loaded with Nd(III) is shown in Table S1.† It is evident that 0.001 M HNO_3 also exhibits the best stripping efficiency.

Table 2 Thermodynamic data of Nd extraction reaction using L^I and L^{II} ligands, $[Nd^{3+}]_{init}$ = 3 mM, $[L^I/L^{II}]$ = 0.024 M, $[HNO_3]$ = 3 M

Species	ΔH (kJ mol^{-1})	ΔS (J mol^{-1})	ΔG (298 K) (kJ mol^{-1})	log K (298 K)
L^I–Nd[26]	−33.20	−32.53	−23.51	4.13
L^{II}–Nd	−22.82	−24.69	−15.46	4.08

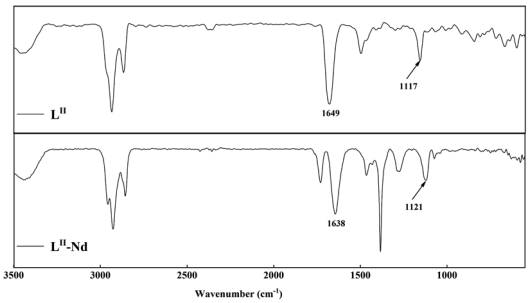

Fig. 7 The FT-IR spectra of ligand L^{II} and its extraction complex.

Infrared spectroscopy studies. The FT-IR spectra of pure L^{II} ligand and the organic phase loaded with Nd(III) were analyzed, as shown in Fig. 7. For the organic phase containing $Nd(NO_3)_3 \cdot 3L^{II}$, the coordinated C=O absorption band is blue-shifted from its position in the pure L^{II} ligand spectrum at 1649 cm^{-1} to 1638 cm^{-1}. The asymmetric stretching vibration band of the ether bond is locates at 1117 cm^{-1}. After complexing with the metal ions, the absorption band of the ether bond is red-shifted to 1121 cm^{-1}. This suggests that the L^{II} molecule might form a tridentate complex with Nd(III) through two carbonyl groups and one ether group.[60,61]

Third phase formation

Fig. 8 exhibits the LOC and CAC of nitric acid depending on the concentration of *n*-octanol. LOC and CAC increase with an increase in the *n*-octanol concentration, which is consistent with previous results.[9,10,62] The variation in the LOC and CAC of

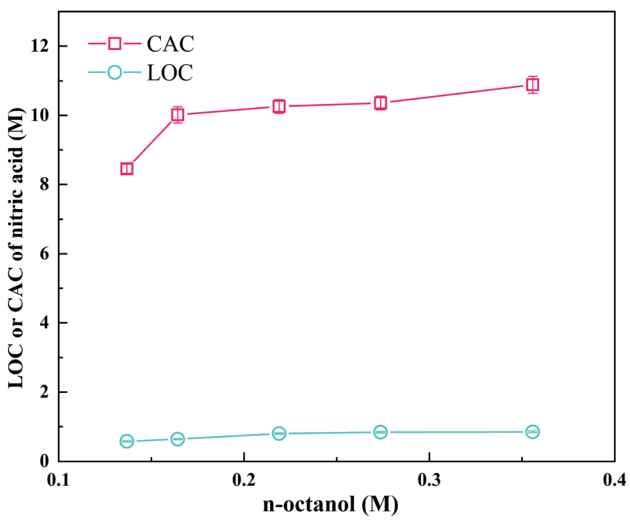

Fig. 8 LOC and CAC of nitric acid as a function of *n*-octanol concentration, $[L^{II}]$ = 0.12 M.

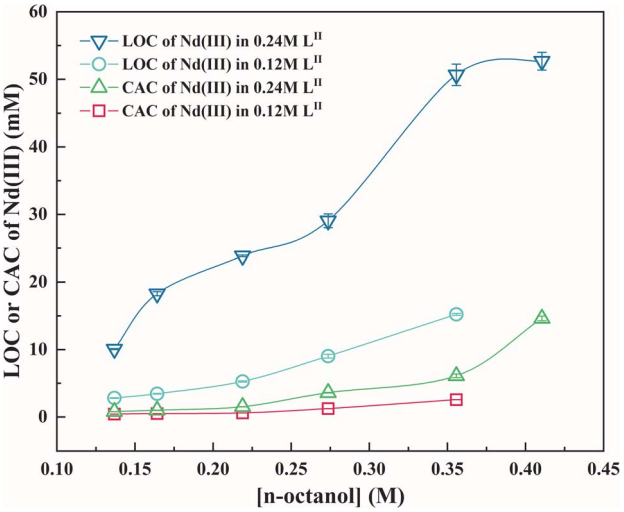

Fig. 9 LOC and CAC of Nd(III) as a function of *n*-octanol concentration.

Nd(III) in L^{II} with *n*-octanol concentration at 298 K for two different concentrations are shown in Fig. 9. It was found that *n*-octanol, as a phase modifier, effectively inhibited the third phase formation; moreover, at the same *n*-octanol concentration, the LOC and CAC of Nd(III) in the 0.24 M L^{II} system are larger than those in the 0.12 M L^{II} system. Generally, the formation of the third phase is owing to the increased polarity of the complexes after the Nd ions be extracted, which decreases their solubility in the non-polar diluent.[27] Therefore, the degree of solvation of the complexes increase with the increasing of the *n*-octanol concentration.

Fig. S4 and S5† show the trends of the LOC of Nd(III) with the initial HNO_3 acidity and L^{II} concentration, respectively. The LOC values decrease with an increasing of the nitric acid concentration on account of the competition between nitric acid and Nd(III)[26] and increase with an increasing of the concentration of the extractant. When HNO_3 or Nd(III) is transferred from the aqueous phase to the organic phase, acid-solvates, such as $DGA\cdot(HNO_3)_x$, and metal-solvates, such as $DGA\cdot(Nd(NO_3)_3)_x$, are formed.[63,64] The solvent molecules have strong polarity and tend to interact with each other automatically and undergo self-aggregation, thus forming spherical reverse micelles at mesoscopic scales.[65] The tendency of aggregation depends on the polarity of the functional groups and the van der Waals interaction between the alkyl groups of the ligand and diluent.[66,67] Typically, these reverse micelles have a structure with the metal ion as the core surrounded by long-chain alkyl groups. Table 3 presents the LOC and CAC of Nd in the L^{I} and L^{II} solvent systems. In general, compared with the L^{II} ligand, the L^{I} ligand have lower CAC values and higher LOC values. The higher LOC of L^{I} means that the extraction capability of L^{I} was better than L^{II}, and the lower CAC value means that it is easier to form the third phase in L^{I} than L^{II}.

Table 3 Comparison of CAC and LOC values of Nd(III) in *n*-octanol/kerosene at 298 K

	Ligand	L^{I}		L^{II}	
[L] (M)	[*n*-octanol] (M)	CAC (mM)	LOC (mM)	CAC (mM)	LOC (mM)
0.024	0.14	0.30	3.73	0.42	2.81
	0.22	0.46	7.05	0.60	5.27
	0.27	1.06	12.09	1.23	9.02

Theory Calculations

Geometrical and electronic structures of the ligands. The electrostatic potential (ESP) diagrams for the L^{I} and L^{II} ligands are presented in Fig. 10. The molecular geometries of the two ligands were optimized at the theoretical level B3LYP/6-311G(d) in the gas phase. The red and blue regions indicate the local maximum/minimum and positive/negative potentials, respectively. The negative electrostatic potential corresponds to the enrichment of electrons, and electron-rich positions are the preferred sites for Nd(III) coordination.[68,69]

As shown in Fig. 10, there are minimum electrostatic potential points close to the ether O atom denoted as O_{ether} and the two amide O atoms denoted as O_{amide1} and O_{amide2}. For the L^{I} ligand, the ESP values of O_{amide1} and O_{amide2} atoms are -40.30 and -40.11 kcal mol^{-1}, respectively. For the L^{II} ligand, O_{amide1} is connected with two octyl groups, and its ESP value is -41.47 kcal mol^{-1}, and O_{amide2} is connected with two methyl groups, and the corresponding ESP value is -37.59 kcal mol^{-1}. It is clear that for both L^{I} and L^{II} ligands, O_{amide1} and O_{amide2} have more negative electrostatic potentials than O_{ether}; thus, the two amide O atoms are more likely to coordinate with the metal ions than the ether O atom. In addition, the difference between the ESP values of O_{amide1} and O_{amide2} in L^{II} is larger than that in L^{I}. In general, long-chain alkyl groups have a stronger electron-donating inductive effect than short alkyl chains, leading to a larger electron density on the amide O atom adjacent to the long alkyl chains. Therefore, the ESP value of O_{amide1} is more negative than that of O_{amide2} in L^{II}, and the ESP values of O_{amide1} and O_{amide2} are approximately identical in L^{I}.

The Mulliken charges on the O_{ether} and O_{amide} of L^{I} and L^{II} are shown in Table S2.† The Mulliken charges on O_{ether} of the two ligands are the same and less than those on the two amide O atoms. For L^{I}, the Mulliken charges on O_{amide1} and O_{amide2} are the same, whereas, for L^{II}, the Mulliken charge on O_{amide1} is larger than that on O_{amide2}, which would affect the interaction

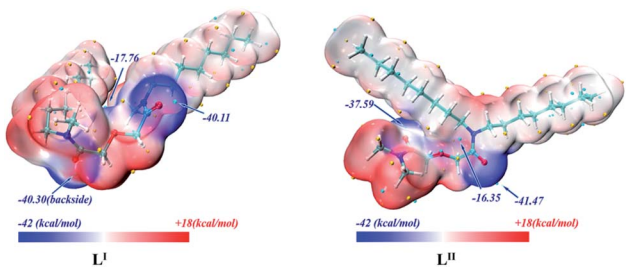

Fig. 10 ESP plots of the optimized L^{I} and L^{II} ligands.

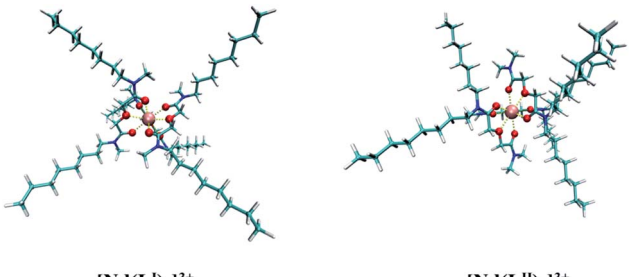

Fig. 11 Optimized structures of $[Nd(L^{I})_3]^{3+}$ and $[Nd(L^{II})_3]^{3+}$ at the B3LYP/6-3111G(d)/RECP level of theory in the gas phase. The H, C, N, O, and Nd atoms are represented by white, cyan, blue, red and pink, respectively.

between these ligands and metal ions, and further affect the stability of the complexes.

Optimized structures of the $[NdL_3]^{3+}$ complexes. It has been reported that when DGA ligands complex with Ln(III) from the nitric acid medium, the nitrate ions do not directly bond to the Ln(III) centers in the solvent extraction system but rather act as counterions in the form of ion pairs to balance the positive charge of the 1 : 3 complexes.[70–72] The geometries of the two complexes were optimized at the B3LYB/6-311G(d)/RECP level of theory in the gas phase, and the structures are shown in Fig. 11. They indicated that both ligands coordinate with the Nd(III) ion acting as the tridentate type. Table S3† lists the bond lengths between Nd(III) and the ether O atom and the two amide O atoms of L^{I} and L^{II}. In both L^{I} and L^{II}, the O_{ether}–Nd bond lengths are longer than the O_{amide1}–Nd and O_{amide2}–Nd bond lengths. The bond length of O_{amide1}–Nd is almost identical to that of O_{amide2}–Nd in L^{I}, and the bond length of O_{amide2}–Nd is shorter than that of O_{amide2}–Nd in the L^{II} ligand; therefore, there are some differences in the complexation strength between the two amide O atoms and Nd(III) in the L^{II} ligand.

Bonding nature and topological analysis of the complexes. Mayer bond orders (MBOs) of the Nd–O bonds were calculated and are presented in Table 4.[73,74] MBOs were within the 0.113–0.325 range, indicating that the interactions between the ligands and the metal ions display weak covalency. MBOs between O_{amide1}–Nd and O_{amide2}–Nd in L^{I} are almost the same, while the MBOs of O_{amide1}–Nd and O_{amide2}–Nd in L^{II} are different. Besides, the average value of the MBOs of O_{amide1}–Nd and O_{amide2}–Nd in L^{I} is slightly larger than that in L^{II}, which

Table 4 Calculated MBOs of the O_{ether}–Nd and O_{amide}–Nd bonds in the $[NdL_3]^{3+}$ complexes at the B3LYB/6-311G(d)/RECP level of theory

Ligand	Bond	MBOs				Average
L^{I}	O_{ether}–Nd	0.113	0.114	0.113	0.113	0.319
	O_{amide1}–Nd	0.318	0.319	0.318	0.319	
	O_{amide2}–Nd	0.320	0.319	0.318	0.319	
L^{II}	O_{ether}–Nd	0.113	0.116	0.115	0.114	0.317
	O_{amide1}–Nd	0.311	0.312	0.308	0.310	
	O_{amide2}–Nd	0.322	0.325	0.325	0.324	

Table 5 Calculated topological properties (a.u.) at the M–O_{amide} and M-O_{ether} BCPs in the $[NdL_3]^{3+}$ complexes at the B3LYB/6-311G(d)/RECP level of theory

	Species			
	$[NdL_3^{I}]^{3+}$		$[NdL_3^{II}]^{3+}$	
Bond type	$\rho(r)$	$\nabla^2\rho(r)$	$\rho(r)$	$\nabla^2\rho(r)$
O_{amide1}–Nd	0.048	0.195	0.050	0.201
	0.048	0.194	0.049	0.199
	0.048	0.194	0.050	0.202
O_{amide2}–Nd	0.048	0.194	0.047	0.190
	0.048	0.195	0.047	0.189
	0.048	0.194	0.047	0.190
O_{ether}–Nd	0.029	0.124	0.029	0.123
	0.029	0.124	0.029	0.125
	0.029	0.125	0.028	0.123
Average	0.0461		0.0459	

mean that the coordination bond between L^{I} and Nd(III) was more stable.

Topological analysis based on the electronic wave function information was also performed as part of QTAIM using Multiwfn 3.7, which has already been widely applied in the analysis of the Ln(III)/An(III) complexes. The topological analysis of electron density $\rho(r)$ and its Laplacian ($\nabla^2\rho(r)$) provides information about the bond properties. The (3, −1) saddle point on the electron density curvature is the bond critical point (BCP), and the electron curvature is positive in the direction of the atomic interaction line and negative in the direction of its orthogonality, and the electron density $\rho(r)$ and potential energy density $V(r)$ at the BCP position are closely related to the strength of the chemical bond.[20] Generally, BCP $\rho(r) > 0.20$ a.u. and a negative $\nabla^2\rho(r)$ value represent a covalent (open-shell) interaction, while $\rho(r) < 0.10$ a.u. with a positive $\nabla^2\rho(r)$ value corresponds to a closed-shell interaction, which can be considered as ionic, hydrogen or van der Waals interaction. As shown in Table 5, the $\rho(r)$ values at the O_{amide}–Nd and O_{ether}–Nd BCPs are <0.1 a.u., and all the $\nabla^2\rho(r)$ values are positive. Therefore, the interactions between the two ligands and Nd(III) show the mainly ionic characteristics.

In addition, the $\rho(r)$ values at the O_{amide1}–Nd BCP for the two complexes are larger than those at Nd–O_{ether}, demonstrating that O_{amide} have a stronger capacity for complexation. The slightly larger difference between the $\rho(r)$ values at the O_{amide1}–Nd and O_{amide2}–Nd of the L^{II} ligand combined with the results on MBOs and electrostatic potential prove that the interactions between the two O_{amide} of L^{II} and Nd(III) are in a state of imbalance. The average $\rho(r)$ value at the Nd-O_{amide} BCP of $[NdL_3^{I}]^{3+}$ is larger than that of $[NdL_3^{II}]^{3+}$, further showing that there is a stronger interaction between Nd(III) and the L^{I} ligand.[75]

Thermodynamic analysis. The theoretically calculated Gibbs free energy (ΔG) at the M05-2X/6-31G(d)/SMD level for the reactions between L^{I}/L^{II} and Nd(III) are shown in Table 6. The values of ΔG for the two reactions are both negative, which

Table 6 Calculated changes in the Gibbs free energies (kJ mol^{-1}) of the reactions of the Nd(III) complexes

Reactions	ΔG (298 K)
$[Nd(H_2O)_9]_{(aq)}^{3+} + L^{I}_{(org)} = [NdL^{I}_3]_{(org)}^{3+} + 9H_2O_{(aq)}$	−211.35
$[Nd(H_2O)_9]_{(aq)}^{3+} + L^{II}_{(org)} = [NdL^{II}_3]_{(org)}^{3+} + 9H_2O_{(aq)}$	−181.87

prove that the coordination reaction proceeded spontaneously. The calculated free energy for the formation of the 1 : 3 Nd(III)/L^{I} complex (−211.35 kJ mol^{-1}) is more negative than that of 1 : 3 Nd(III)/L^{I} complex (−181.87 kJ mol^{-1}), which is in good agreement with the order of the experimentally determined distribution ratio values. This further verify that L^{I} possesses outstanding complexing ability with Nd(III) than L^{II}.

Conclusions

In the present study, *N*,*N*-dimethyl-*N*′,*N*′-dioctyl diglycolamide (L^{II}) was synthesized, and its extraction and loading capabilities towards Nd(III) from the nitric acid medium were studied by employing 40/60 (v/v)% *n*-octanol/kerosene as the diluent. D_{Nd} increases with nitric acidity and the concentration of the extractant and decreases with increasing temperature. The stoichiometry of the extracted species is $Nd(NO_3)_3 \cdot 3L^{II}$, as verified by the results of ESI-MS and FT-IR. The LOC and CAC of Nd increase with the increasing in the concentrations of *n*-octanol and extractant and decreased with the increase in the initial acidity of the aqueous medium. In comparison with its isomeric ligand *N*,*N*′-dimethyl-*N*,*N*′-dioctyl diglycolamide (L^{I}), L^{II} shows a lower distribution ratio of Nd(III) but is more advantageous in terms of preventing the formation of the third phase, which is reflected in its higher CAC value under similar experimental conditions.

The electrostatic potential and Mulliken charge analysis of the two ligands indicate that the difference in the electron-donating ability of the two amide O atoms in L^{II} is larger than that in L^{I}. The complexation between L^{I}/L^{II} and Nd(III) is predominantly through ionic interactions. The MBOs and QTAIM show that the complexation interaction strength of Nd–O_{amide1} and Nd–O_{amide2} are almost identical in L^{I}, while those in L^{II} display certain differences, and this inhomogeneity in L^{II} seem to influence its extraction performance towards metal ions, such as Nd(III), which is in accordance with the thermodynamic results. These results may shed light on the design of DGA class ligands for separating HLLW and help us better understand the structure–activity relationship in DGAs.

Conflicts of interest

There are no conflicts to declare.

Acknowledgements

The work was supported by Special Fund of Central University Basic Scientific Research Fee (3072019CF1503).

Notes and references

1 M. Salvatores, *Nucl. Eng. Des.*, 2005, **235**, 805–816.
2 S. A. Ansari, P. K. Mohapatra, A. Leoncini, S. M. Ali, J. Huskens and W. Verboom, *Inorg. Chem.*, 2019, **58**, 8633–8644.
3 S. Tachimori, Y. Sasaki and S. Suzuki, *Solvent Extr. Ion Exch.*, 2007, **20**, 687–699.
4 S. Nave, G. Modolo, C. Madic and F. Testard, *Solvent Extr. Ion Exch.*, 2004, **22**, 527–551.
5 H. Suzuki, Y. Sasaki, Y. Sugo, A. Apichaibukol and T. Kimura, *Radiochim. Acta*, 2004, **92**, 463–466.
6 S. Manohar, J. N. Sharma, B. V. Shah and P. K. Wattal, *Nucl. Sci. Eng.*, 2017, **156**, 96–102.
7 D. Whittaker, A. Geist, G. Modolo, R. Taylor, M. Sarsfield and A. Wilden, *Solvent Extr. Ion Exch.*, 2018, **36**, 223–256.
8 S. A. Ansari, P. Pathak, P. K. Mohapatra and V. K. Manchanda, *Chem. Rev.*, 2012, **112**, 1751–1772.
9 J. Ravi, K. A. Venkatesan, M. P. Antony, T. G. Srinivasan and P. R. Vasudeva Rao, *J. Radioanal. Nucl. Chem.*, 2012, **295**, 1283–1292.
10 J. Ravi, T. Prathibha, K. A. Venkatesan, M. P. Antony, T. G. Srinivasan and P. R. Vasudeva Rao, *Sep. Purif. Technol.*, 2012, **85**, 96–100.
11 J. Ravi, K. Venkatesan, M. Antony, T. Srinivasan and P. V. Rao, *Radiochim. Acta*, 2014, **102**, 599–607.
12 E. A. Mowafy and D. Mohamed, *Sep. Sci. Technol.*, 2017, **52**, 1006–1014.
13 Z. Wei, C. Lu, Y. Zhou, C. Jiao, M. Zhang, H. Hou, Y. Gao and G. Tian, *J. Radioanal. Nucl. Chem.*, 2019, **323**, 875–884.
14 Q. Liu, J. Zhou, L. Zhu, Y. Zhang, D. Li, S. Yang and G. Tian, *Solvent Extr. Ion Exch.*, 2020, **38**, 485–495.
15 Y. Liu, Z. Liu, C. Zhao, Y. Zhou, Y. Gao and H. He, *Prog. Chem.*, 2020, **2**, 219–229.
16 Y. Liu, C. Zhao, Z. Liu, Y. Zhou, C. Jiao, M. Zhang, H. Hou, Y. Gao, H. He and G. Tian, *J. Radioanal. Nucl. Chem.*, 2020, **325**, 409–416.
17 Q. Chen, C. Lu, Y. Hu, Y. Liu, Y. Zhou, C. Jiao, M. Zhang, H. Hou, Y. Gao and G. Tian, *J. Radioanal. Nucl. Chem.*, 2021, **327**, 565–573.
18 Y. Liu, C.-Z. Wang, Q.-Y. Wu, J.-H. Lan, Z.-F. Chai, Q. Liu and W.-Q. Shi, *Inorg. Chem.*, 2020, **59**, 11469–11480.
19 D. Stamberga, M. R. Healy, V. S. Bryantsev, C. Albisser, Y. Karslyan, B. Reinhart, A. Paulenova, M. Foster, I. Popovs, K. Lyon, B. A. Moyer and S. Jansone-Popova, *Inorg. Chem.*, 2020, **59**, 17620–17630.
20 C. Wang, Q. Y. Wu, C. Z. Wang, J. H. Lan, C. M. Nie, Z. F. Chai and W. Q. Shi, *Dalton Trans.*, 2020, **49**, 4093–4099.
21 S. Guoxin, L. Min, C. Yu, Y. Meilong and Y. Shaohong, *Solvent Extr. Ion Exch.*, 2010, **28**(4), 482–494.
22 A. Suresh, C. V. S. B. Rao, K. N. Sabharwal, T. G. Srinivasan and P. R. V. Rao, *Solvent Extr. Ion Exch.*, 1999, **17**, 73–86.
23 M. Bodanszky, J. C. Tolle, S. S. Deshmane and A. Bodanszky, *Int. J. Pept. Protein Res.*, 2009, **12**, 57–68.
24 Z. Kolarik and E. P. Horwitz, *Solvent Extr. Ion Exch.*, 1988, **6**, 61–91.

25 P. R. Vasudeva Rao and Z. Kolarik, *Solvent Extr. Ion Exch.*, 1996, **14**, 955–993.
26 Y. Liu, Y. Gao, Z. Wei, Y. Zhou, M. Zhang, H. Hou, G. Tian and H. He, *J. Radioanal. Nucl. Chem.*, 2018, **318**, 2087–2096.
27 P. Deepika, K. N. Sabharwal, T. G. Srinivasan and P. R. Vasudeva Rao, *Solvent Extr. Ion Exch.*, 2010, **28**, 184–201.
28 P. John, *Phys. Rev. B: Condens. Matter Mater. Phys.*, 1986, **33**, 8822–8824.
29 R. Nityananda, P. Hohenberg and W. J. R. Kohn, *Resonance*, 2017, **22**, 809–811.
30 M. Frisch, G. Trucks, H. Schlegel, G. Scuseria, M. Robb, J. Cheeseman, G. Scalmani, V. Barone, G. Petersson and H. Nakatsuji, *GAUSSIAN 16 (Revision B.01)*, Gaussian Inc., Pittsburgh, PA, 2016.
31 A. D. Becke, *Phys. Rev. B: Condens. Matter Mater. Phys.*, 1998, **98**, 5648–5652.
32 C. Lee, W. Yang and R. G. Parr, *Phys. Rev. B: Condens. Matter Mater. Phys.*, 1988, **37**, 785.
33 Q. Y. Wu, Y. T. Song, L. Ji, C. Z. Wang, Z. F. Chai and W. Q. Shi, *Phys. Chem. Chem. Phys.*, 2017, **19**, 26969–26979.
34 A. Zaiter, B. Amine, Y. Bouzidi, L. Belkhiri, A. Boucekkine and M. Ephritikhine, *Inorg. Chem.*, 2014, **53**, 4687–4697.
35 M. Dolg, H. Stoll and H. J. Preuss, *J. Chem. Phys.*, 1989, **90**, 1730–1734.
36 W. Küchle, M. Dolg, H. Stoll and H. Preuss, *J. Chem. Phys.*, 1994, **100**, 7535–7542.
37 X. Cao and M. J. T. Dolg, *J. Mol. Struct.*, 2002, **581**, 139–147.
38 Y. Zhao and D. G. Truhlar, *J. Chem. Phys.*, 2008, **128**, 184109.
39 M. Regueiro-Figueroa, D. Esteban-Gómez, A. de Blas, T. Rodríguez-Blas and C. Platas-Iglesias, *Chem.–Eur. J.*, 2014, **20**, 3974–3981.
40 A. J. Bridgeman, G. Cavigliasso, L. R. Ireland and J. Rothery, *Dalton Trans.*, 2001, 2095–2108.
41 R. F. Bader, *J. Chem. Rev.*, 1991, **91**, 893–928.
42 R. F. Bader, *J. Phys. Chem. A*, 1998, **102**, 7314–7323.
43 H.-B. Zhao, M. Zheng, G. Schreckenbach and Q.-J. Pan, *Dalton Trans.*, 2018, **47**, 2148–2151.
44 T. Lu and F. J. Chen, *J. Comput. Chem.*, 2012, **33**, 580–592.
45 F. McLachlan, K. Greenough, A. Geist, B. McLuckie, G. Modolo, A. Wilden and R. Taylor, *Solvent Extr. Ion Exch.*, 2016, **34**, 334–346.
46 J. Ravi, K. A. Venkatesan, M. P. Antony, T. G. Srinivasan and P. R. Vasudeva Rao, *Solvent Extr. Ion Exch.*, 2014, **32**, 424–436.
47 D. Xu, Z. Shah, Y. Cui, L. Jin, X. Peng, H. Zhang and G. Sun, *Hydrometallurgy*, 2018, **180**, 132–138.
48 Y. Xu, Y. Gao, Y. Zhou, C. Fan, H. Hou and M. Zhang, *Solvent Extr. Ion Exch.*, 2017, **35**, 507–518.
49 X. Cai, B. Wei, J. Han, Y. Li, Y. Cui and G. Sun, *Hydrometallurgy*, 2016, **164**, 1–6.
50 K. Pitzer, *J. Phys. Chem.*, 1973, **77**, 268–277.
51 K. S. Pitzer and G. Mayorga, in *Molecular Structure and Statistical Thermodynamics: Selected Papers of Kenneth S. Pitzer*, World Scientific, 1993, pp. 396–404.
52 K. S. Pitzer, *Activity Coefficients in Electrolyte Solutions*, CRC Press, 2018.
53 X. Liu, G. Sun, X. Cai, X. Yang, Y. Li, Z. Sun and Y. Cui, *J. Radioanal. Nucl. Chem.*, 2015, **306**, 549–553.
54 E. A. Mowafy and D. Mohamed, *J. Rare Earths*, 2015, **33**, 432–438.
55 E. A. Mowafy and H. F. Aly, *Solvent Extr. Ion Exch.*, 2007, **25**, 205–224.
56 P. N. Pathak, S. A. Ansari, S. V. Godbole, A. R. Dhobale and V. K. Manchanda, *Spectrochim. Acta, Part A*, 2009, **73**, 348–352.
57 Y. Cai, S. A. Ansari, K. Fu, B. Zhu, H. Ma, L. Chen, S. D. Conradson, S. Qin, H. Fu, P. K. Mohapatra, L. Yuan and W. Feng, *J. Hazard. Mater.*, 2020, 124214, DOI: 10.1016/j.jhazmat.2020.124214.
58 R. B. Gujar, S. A. Ansari, P. K. Mohapatra and V. K. Manchanda, *Solvent Extr. Ion Exch.*, 2010, **28**, 350–366.
59 Y. Cui, Y.-q. Wang, M.-p. Pang, L.-n. Zhang, H.-f. Zhou, Q.-y. Dang and G.-x. Sun, *Hydrometallurgy*, 2015, **152**, 1–6.
60 F. Kou, S. Yang, H. Qian, L. Zhang, C. M. Beavers, S. J. Teat and G. Tian, *Dalton Trans.*, 2016, **45**, 18484–18493.
61 F. Kou, S. Yang, L. Zhang, S. J. Teat and G. Tian, *Inorg. Chem. Commun.*, 2016, **71**, 41–44.
62 J. Ravi, K. A. Venkatesan, M. P. Antony, T. G. Srinivasan and P. R. Vasudeva Rao, *Radiochim. Acta*, 2014, **102**, 609–617.
63 A. Paquet, O. Diat, L. Berthon and P. Guilbaud, *J. Mol. Liq.*, 2019, **277**, 22–35.
64 T. Prathibha, K. A. Venkatesan and M. P. Antony, *Colloids Surf., A*, 2018, **538**, 651–660.
65 R. Ganguly, J. N. Sharma and N. Choudhury, *J. Colloid Interface Sci.*, 2011, **355**, 458–463.
66 P. N. Pathak, S. A. Ansari, S. Kumar, B. S. Tomar and V. K. Manchanda, *J. Colloid Interface Sci.*, 2010, **342**, 114–118.
67 M. P. Jensen, T. Yaita and R. Chiarizia, *Langmuir*, 2007, **23**, 4765–4774.
68 R. G. Surbella III, L. C. Ducati, K. L. Pellegrini, B. K. McNamara, J. Autschbach, J. M. Schwantes and C. L. Cahill, *J. Am. Chem. Soc.*, 2017, **139**, 10843–10855.
69 T. Lu and S. Manzetti, *J. Struct. Chem.*, 2014, **25**, 1521–1533.
70 Y. Gong, G. Tian, L. Rao and J. K. Gibson, *Inorg. Chem.*, 2014, **53**, 12135–12140.
71 G. Tian, S. J. Teat and L. Rao, *Inorg. Chem.*, 2014, **53**, 9477–9485.
72 D. M. Brigham, A. S. Ivanov, B. A. Moyer, L. H. Delmau, V. S. Bryantsev and R. J. Ellis, *J. Am. Chem. Soc.*, 2017, **139**, 17350–17358.
73 I. Mayer, *J. Quantum Chem.*, 1986, **29**, 477.
74 X.-W. Chi, Q.-Y. Wu, Q. Hao, J.-H. Lan, C.-Z. Wang, Q. Zhang, Z.-F. Chai and W.-Q. Shi, *Organometallics*, 2018, **37**, 3678–3686.
75 B. Vlaisavljevich, P. Miro, C. J. Cramer, L. Gagliardi, I. Infante and S. T. Liddle, *Chem. - Eur. J.*, 2011, **17**, 8424–8433.